Nanoparticle Gradient

DOI: 10.1002/anie.201207902

A Simple Route to Hierarchically Assembled Micelles and Inorganic Nanoparticles**

*Wei Han, Myunghwan Byun, Bo Li, Xinchang Pang, and Zhiqun Lin**

Hierarchical assembly of nanoscale materials has attracted considerable attention, as these materials have tremendous potential for applications in optics, photonics, electronics, optoelectronics, magnetic devices, and biotechnology.[1] An intriguing preparative strategy for hierarchical structures is to perform top-down synthesis using bottom-up self-assembling materials.[2] In the latter context, block copolymers have been widely recognized as particularly important materials because they are thermodynamically driven to self-assemble into a wide range of periodic nanoscopic morphologies (e.g., spheres, cylinders, double gyroids, and lamellae), depending on the volume fraction of their components.[3] They offer great promise for the creation of complex and hierarchical assemblies. Interestingly, among various types of block copolymers, when placed in "selective" solvents, amphiphilic linear block copolymers composed of a hydrophobic block and a hydrophilic block have the propensity to form a large number of aggregate structures, for example, spherical inverse micelles consisting of a core of hydrophobic block and a corona of hydrophilic block in an aqueous solution.[4] These micelles are known as polymeric micelles and provide new opportunities for the construction of drug-delivery vehicles, fabrication of complex assemblies with controlled size and shape,[5] and creation of inorganic nanoparticles for use in, for example, catalysis and solar cells.[6]

Drying-mediated self-assembly of a droplet containing nonvolatile solutes (i.e., nanoparticles, colloids, and polymers) is an emerging surface-patterning technique that yields intriguing structures.[7] However, the structures formed are often irregular and stochastically organized, rather than uniform structures. To date, only a few studies have shown precise control over the evaporation process (e.g., evaporative flux, solution concentration, and interfacial interaction between the solute and substrate) to yield complex structures and assemblies with high regularity and fidelity by forcing the drying droplet to evaporate in a restricted geometry,[8] including "curve-on-flat" geometry,[8a–g] two-plate geometry,[9] and cylindrical tube.[10] These confined geometries allow for exquisite control over the flow within the drying droplet, which in turn promotes the formation of highly ordered structures, dispensing with the need for lithography techniques and external fields.

Herein, we demonstrate one-step hierarchical assembly of an amphiphilic diblock copolymer (poly(styrene)-*block*-poly(4-vinylpyridine) (PS-*b*-P4VP)) micelles using a gradient method by combining two distinct self-assembling processes at different scales, namely, a top-down controlled evaporative self-assembly (CESA) of a PS-*b*-P4VP solution confined to the "cylinder-on-Si" geometry on the microscopic scale and a bottom-up self-assembly of PS-*b*-P4VP micelles into regular arrays on the nanometer scale. The surface reconstruction of hierarchically arranged micelles led to the formation of nanoporous arrays when they were immersed in a solvent that is selective for the P4VP block. Remarkably, hierarchical assembly of microscopic Au stripes, containing 2D arrays of Au nanoparticles in the stripes, were also produced by CESA of the PS-*b*-P4VP/precursor solution, followed by exposure to oxygen plasma that facilitated the reduction of metal ions to Au and the removal of the PS-*b*-P4VP micelle template. This route to hierarchically assembled micelles and inorganic nanoparticles is simple and easy to implement, giving a high yield over large areas at low cost. This strategy represents a significant advance over other processes that rely on many fabrication steps with expensive instrumentation to assemble block copolymers and nanoparticles into hierarchical structures.

The diblock copolymer, PS-*b*-P4VP was used as a nonvolatile solute and dissolved in toluene at a concentration of 0.1 mg mL^{-1} (see Experimental Section). A drop of PS-*b*-P4VP toluene solution was loaded and confined in an axially symmetric geometry composed of a cylindrical lens on a Si substrate. (i.e., the cylinder-on-Si geometry shown in Figure 1a), leading to a polymer solution held in place by capillary action with the highest evaporation rate at its extremity. As toluene evaporated from the edge of the solution, it triggered the pinning of the three-phase contact line (i.e., "stick") by transporting PS-*b*-P4VP chains from the interior of the solution. During the deposition of PS-*b*-P4VP (i.e., pinning), the initial contact angle of the meniscus gradually decreased to a critical value owing to the evaporative loss of toluene, at which the capillary force (i.e., depinning) became larger than the pinning force.[8f] This caused the contact line to move toward the cylinder/Si contact center (arrows within the confined PS-*b*-P4VP solution; lower left panel in Figure 1a) and stop at a new position (i.e., "slip"), leaving behind a local stripe. Repeated pinning and depinning cycles of the contact line led to the formation of

[*] Dr. W. Han, B. Li, Dr. X. Pang, Prof. Z. Lin
School of Materials Science and Engineering
Georgia Institute of Technology, Atlanta, GA 30332 (USA)
E-mail: zhiqun.lin@mse.gatech.edu
Dr. M. Byun
Department of Polymer Science and Engineering
University of Massachusetts, Amherst, MA 01002 (USA)

[**] We gratefully acknowledge support from the National Science Foundation (NSF CBET-1153660 and CMMI-1153663) and the Georgia Institute of Technology.

Supporting information for this article is available on the WWW under http://dx.doi.org/10.1002/anie.201207902.

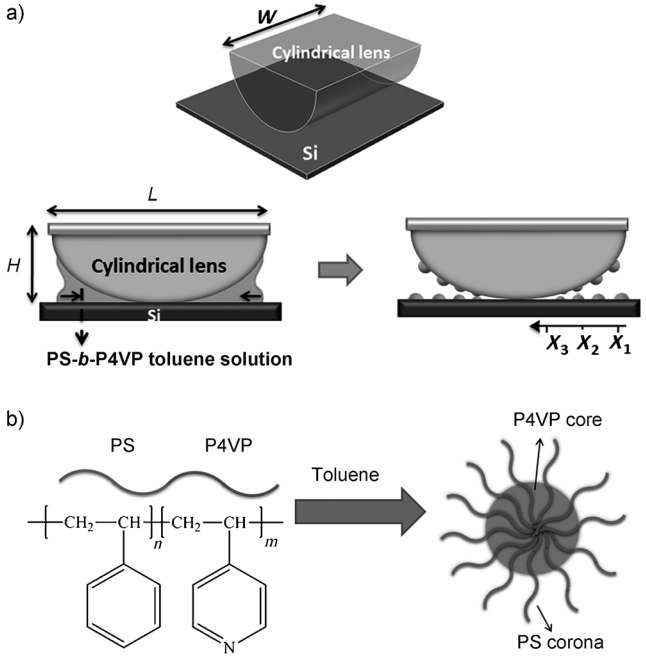

Figure 1. a) Scheme of the formation of highly ordered PS-*b*-P4VP stripes in a gradient. A drop of PS-*b*-P4VP toluene solution was trapped in a confined geometry consisting of a cylindrical lens situated on a flat Si substrate (3D view; upper panel), held in place by capillary action (side view; lower panels). *H*, *L*, and *W* are the height, length, and width of the cylindrical lens, respectively. The black arrows on both sides of the cylinder-on-Si geometry mark the movement of the solution front toward the cylinder/Si contact center (lower left panel). X_n ($n=1$–3) is the distance from the first deposit toward the cylinder/Si contact center. b) Chemical formula of PS-*b*-P4VP, and scheme of the formation of PS-*b*-P4VP micelle in toluene.

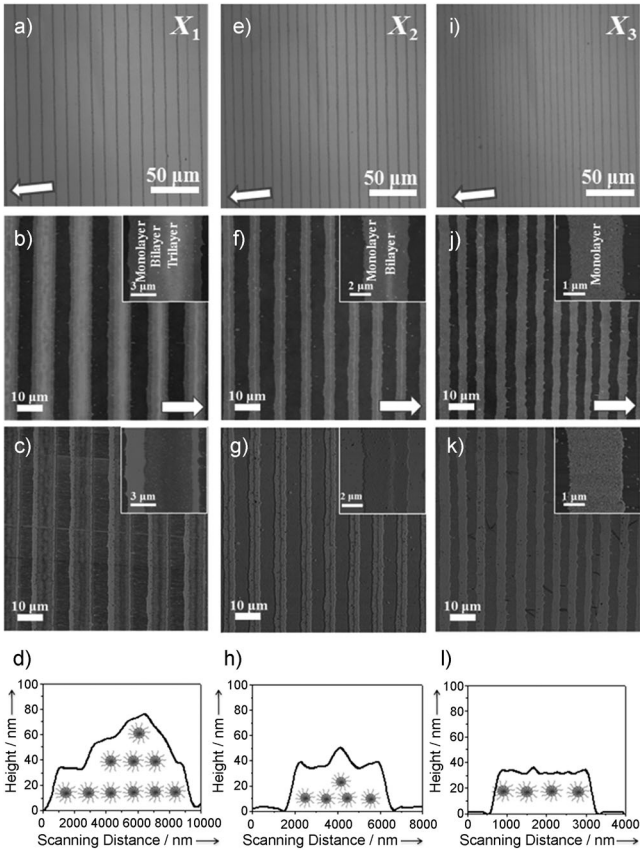

Figure 2. Optical micrographs (a,e,i), AFM height images (b,f,j)and phase images (c,g,k), and the corresponding height profiles (d,h,l) for the PS-*b*-P4VP stripes formed by CESA in the cylinder-on-Si geometry at a–d) $X_1=4500$ μm; e–h) $X_2=4000$ μm; and i–l) $X_3=3500$ μm. The arrows in the optical micrographs and AFM images mark the movement of the solution front during evaporation. *Z* range = 200 nm in all AFM height images.

regular stripes of PS-*b*-P4VP with a global gradient, guided by the shape of the upper cylindrical lens (lower right panel in Figure 1 a).

After complete toluene evaporation, the PS-*b*-P4VP stripes deposited on the Si substrate were examined with optical microscopy (OM) and atomic force microscopy (AFM), revealing the formation of highly ordered gradient stripes over the entire surface of the Si substrate, except in the region where the cylindrical lens was in contact with the Si surface. The representative optical micrographs and AFM images at the different regions, X_n are shown in Figure 2. X_n is the distance from the first deposit toward the cylinder/Si contact center (lower right panel in Figure 1 a). The width, *w*, and height, *h*, of the stripes as well as the center-to-center distance, $\lambda_{c\text{-}c}$ between adjacent stripes were found to decrease with increased proximity to the cylinder/Si contact center (Figure 2 a,e,i; from X_1 to X_2 to X_3). Close examination of the stripes by AFM clearly showed that the stripes progressively decreased from $w=8.2$ μm, $h=74.4$ nm, and $\lambda_{c\text{-}c}=16.2$ μm at the outermost region ($X_1=4500$ μm; Figure 2 b,c) to $w=4.2$ μm, $h=54.6$ nm, and $\lambda_{c\text{-}c}=11.9$ μm at the intermediate region ($X_2=4000$ μm; Figure 2 f,g) to $w=2.7$ μm, $h=35.2$ nm, and $\lambda_{c\text{-}c}=7.6$ μm at the innermost region ($X_3=3500$ μm; Figure 2 j,k). The formation of these microscopic stripes resulted from competition between the linear pinning force and nonlinear capillary force,[8f] as the evaporation of toluene proceeded in the cylinder-on-Si geometry. Remarkably, the formation of gradient PS-*b*-P4VP stripes was highly reproducible.

As toluene is strongly selective for PS, PS-*b*-P4VP diblock copolymers would spontaneously associate into nanoscopic spherical micelles with a soluble PS corona and an insoluble P4VP core to reduce energetically unfavorable interactions between the P4VP blocks and toluene (Figure 1 b).[11] In general, the radius of PS-*b*-P4VP micelles in toluene, R_c can be calculated by Equation (1):[12]

$$4\pi R_c^{\,3}/3 = Z N_A \nu_0 \quad (1)$$

where ν_0 is the molar volume of the core monomer; *Z* is the aggregation number defined by $Z_0(N_A{}^{\alpha} N_B{}^{-\beta})$; and N_A and N_B are the degree of polymerization of the insoluble P4VP core and the soluble PS corona, respectively. Given that $Z_0=1.66$, $\alpha=1.93$, $\beta=0.79$ for the PS-*b*-P4VP/toluene system,[12] $N_A=228$, and $N_B=394$, the R_c of PS-*b*-P4VP micelles in the present study was found to be 17.2 nm. Thus, the PS-*b*-P4VP stripes formed a monolayer, bilayer, and trilayer at three different regions, that is, monolayer, bilayer, and trilayer ($h_{trilayer}=74.4$ nm) at X_1, monolayer and bilayer ($h_{bilayer}=$

54.6 nm) at X_2, and monolayer only ($h_{monolayer} = 35.2$ nm) at X_3, as shown in Figure 2 d,h,l, respectively. The values of h in different X_n regions ($n = 1$–3) were obtained from the cross-sectional scan of AFM height images shown in the insets of Figure 2 b,f,j. The large value of h implied a longer pinning time of PS-*b*-P4VP micelles at the three-phase contact line and a large amount of micelles transported to the contact line (X_1, where in conjunction with the trilayer seen in the center of the stripe, the formation of bilayer and monolayer of PS-*b*-P4VP were also clearly evident (inset in Figure 2 b)). As the toluene evaporated, fewer micelles were available to pin at the contact line as the meniscus moved toward the cylinder/Si contact center, thereby leading to a decreased stripe height (X_2, where in conjunction with the bilayer formed in the center of the stripe, a monolayer of PS-*b*-P4VP was also observed (inset in Figure 2 f)); and ultimately, forming a monolayer at the innermost region (X_3).

Further scrutiny of the surface morphologies of an individual PS-*b*-P4VP stripe formed at the different regions (i.e., X_1–X_3) by AFM clearly revealed that nanoscopic PS-*b*-P4VP micelles were self-assembled into closely packed arrays within the stripe. Clearly, hierarchically assembled PS-*b*-P4VP micelles were obtained, that is, a gradient of microscopic stripes formed by CESA were composed of nanoscopic PS-*b*-P4VP micelles, spontaneously self-assembled within the stripes. Interestingly, the micelles in the monolayer within the stripe at X_1–X_3 had a diameter of 35.6 nm (Figure 3), which correlated well with the results calculated based on Equation (1). However, the micelles were relatively smaller (27.2 nm) for the bilayer and trilayer within the stripe (see Supporting Information, Figure S1 a,b,c); this was likely because of the compression of the upper layers of micelles (i.e., bilayer and trilayer) into the monolayer on the Si substrate, making them appear smaller when measured by AFM. This also explained why the height of the bilayer ($h_{bilayer} = 54.6$ nm) and trilayer ($h_{trilayer} = 74.4$ nm) were smaller than twice (approximately 68.8 nm) and three times (approximately 103.2 nm) of the calculated monolayer. In subsequent experiments, we focused on the stripes formed at the innermost region (X_3) that exhibited uniform monolayer-thick surface patterns.

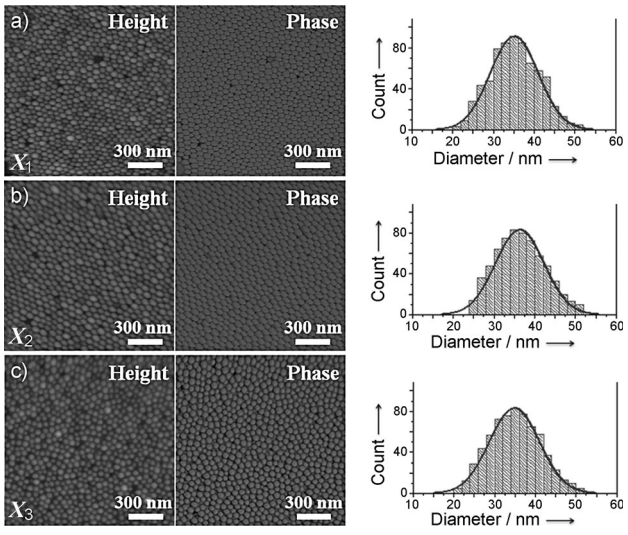

Figure 3. Representative AFM height and phase images, and the corresponding distribution of micelle diameters formed in the monolayer area, as marked in the insets of Figure 2 b,f,j, within the stripe at the three different regions. a) X_1, b) X_2, and c) X_3. Representative AFM height and phase images from the bilayer and trilayer areas within the stripe at X_1, X_2, and X_3 are shown in Figure S1. Z range = 100 nm in all AFM height images.

When the as-prepared PS-*b*-P4VP stripes were exposed to the vapor of tetrahydrofuran (THF), it promoted the ordering of PS-*b*-P4VP micelles. After exposure to THF vapor under argon at room temperature for six hours, a hexagonal array of micelles with improved lateral order was produced, as evidenced by a Fourier-transformed pattern (white dashed square, Figure S2 c). After the vapor annealing, the average micelle diameter decreased from 35.2 nm to 31.8 nm, and the diameter distribution of solvent-annealed micelles was sharpened (right panel, Figure S2 e), compared to the as-prepared stripes (left panel, Figure S2 e). The decreased diameter of micelles may originate from a decrease in the number of diblock copolymer molecules per micelle during the THF vapor annealing.[5b] As P4VP has better solubility in THF than toluene, the redistribution of copolymer chains may occur during the vapor annealing, thus achieving the equilibrium state of micelles with smaller size, narrow size distribution, and improved ordering.[13] We note that the ordering of micelles within the stripes was still short-ranged, which is likely due to the presence of defects (e.g., vacancies between micelles) in the stripes formed during the controlled evaporative self-assembly (CESA) process.

Interestingly, when the as-prepared stripes were immersed in ethanol for 20 minutes, which is a good solvent for P4VP and not a solvent for PS, surface reconstruction of stripes was observed with the emergence of an array of nanopores (Figure S3). The P4VP cores in PS-*b*-P4VP micelles were swollen preferentially by ethanol and subsequently diffused to the top of the PS matrix, creating pores at the position of the P4VP cores[5a,14] (Figure S3 e). Notably, the reconstruction by ethanol to form nanopores did not change the characteristic distance between the adjacent P4VP cores (approximately 45.3 nm), which is in good agreement with the value of the as-prepared sample (approximately 44.9 nm).

Recently, a variety of nanoparticles have been synthesized using PS-*b*-P4VP micelles as a nanostructured template in which the metal salts, as the precursors of nanoparticles, can be selectively coordinated to the P4VP cores.[11a,b,15] We used tetrachloroauric acid ($HAuCl_4 \cdot 3H_2O$) as the precursor of Au nanoparticles. When mixing with the PS-*b*-P4VP toluene solution, the precursors were selectively incorporated into the P4VP cores. The Au^{3+} ions can readily attach to the pyridine groups of P4VP by protonating the pyridine units through ionic–polar interactions.[6b,15a,16] Subsequently, the PS-*b*-P4VP/$HAuCl_4 \cdot 3H_2O$ toluene solution was loaded in the cylinder-on-Si geometry (Figure 1 a). Likewise, the controlled evaporative self-assembly of confined PS-*b*-P4VP/$HAuCl_4 \cdot 3H_2O$ toluene solution yielded highly regular micrometer stripes composed of PS-*b*-P4VP micelles with $HAuCl_4$ encapsulated within the P4VP cores (i.e., PS-*b*-P4VP/$HAuCl_4$ micelles).

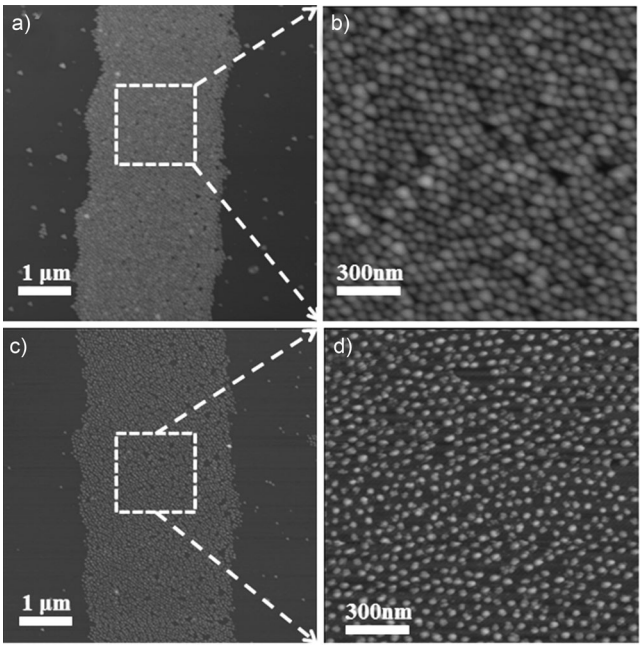

Figure 4. Representative AFM height images of a,c) the monolayer stripes and b,d) the array of micelles within the stripe, a,b) before and c,d) after exposure to oxygen plasma. *Z* ranges are in a) 200 nm, b) 100 nm, c) 50 nm, and d) 50 nm.

Figure 4a,b show the AFM height images of an as-prepared individual micrometer stripe and the array of PS-*b*-P4VP/$HAuCl_4$ micelles on the nanometer scale, respectively, bearing strong resemblance to the pure PS-*b*-P4VP micelles displayed in Figure 3. To make arrays of Au nanoparticles, well-ordered stripes containing PS-*b*-P4VP/$HAuCl_4$ micelles were treated with oxygen plasma for 45 minutes (Figure 4c,d). Upon the exposure to oxygen plasma, the Au^{3+} ions were reduced to elemental Au atoms, owing to a reduction reaction facilitated by 1) the intermediate oxidation product of the polymer (e.g., carbon monoxide; CO) formed during the oxygen plasma exposure, and 2) the electrons from oxygen plasma.[15b,17] At the same time, the PS-*b*-P4VP template was removed by oxygen plasma. Obviously, the Au nanoparticles had a much smaller diameter (approximately 9.8 nm; Figure 4d) as compared to the as-prepared PS-*b*-P4VP/$HAuCl_4$ micelles (approximately 35.2 nm; Figure 4b). Moreover, in comparison to the stripes before the treatment (Figure S4a), the height of stripes after the oxygen-plasma exposure decreased considerably (Figure S4b). The decrease in the diameter and height of surface patterns was most likely due to condensation as a result of the removal of the P4VP cores.[11b] However, the spacing of the patterns after the treatment remained almost the same, with an average value of 45.8 nm, indicating the original order of the micelles was preserved, even after the polymer matrix was removed. The field emission scanning electron microscopy (FESEM) images of the Au stripes and the array of Au nanoparticles within the stripe are shown in Figure S5; they appeared bright, coinciding well with the AFM image (Figure 4d).

To further substantiate the formation of Au nanoparticles by using amphiphilic PS-*b*-P4VP micelles as a template, the samples were monitored by X-ray photoelectron spectroscopy (XPS) before and after exposure to oxygen plasma (Figure 5). Before the oxygen-plasma treatment, as the P4VP cores were simply loaded with the precursor, peaks for elemental Au were not seen (top curve; Figure 5a). After exposure to oxygen plasma, the characteristic peaks of Au $4d_{3/2}$ and $4d_{5/2}$ at binding energies of 353.0 eV and 334.0 eV, respectively, were clearly visible (bottom curve; Figure 5a). The presence of a carbon atom peak following oxygen-plasma treatment (i.e. C 1s) may be due to organic contamination during transfer of the samples from the oxygen plasma for the XPS measurement. Importantly, when performing the XPS scan on the gradient Au stripes, by focusing on the Au $4f_{5/2}$ and $4f_{7/2}$ peaks at binding energies of 87.7 eV and 84.0 eV, respectively, from the outermost region (X_1) to the innermost region (X_3), the intensities of the two Au 4f peaks were seen to decrease progressively (Figure 5b). This decrease correlates well with the decreased nanoparticle thickness from the multilayer region at X_1 to the monolayer region at X_3, similar to the pure PS-*b*-P4VP micelles in Figure 2. The 3D view of the XPS scan, by concentrating on the Au 4f peaks (Figure S6), corroborated that the Au stripes formed in a gradient over large areas, from X_1 to X_3 on both sides of the cylinder-on-Si geometry. It is not surprising that no Au signals were detected in the cylinder/Si contact center because no PS-*b*-P4VP/$HAuCl_4$ micelles were deposited at the contact center, which in turn meant no Au stripes were formed.

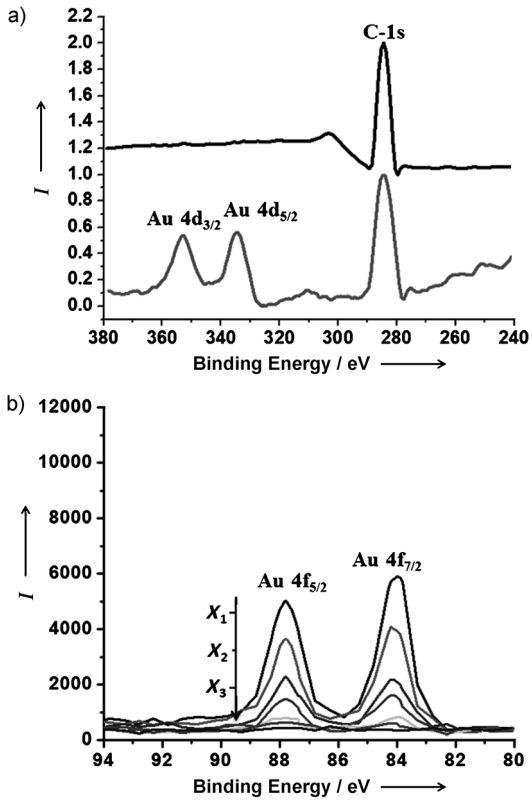

Figure 5. a) XPS spectra for Au-incorporated PS-*b*-P4VP micelles before (top) and after (bottom) the oxygen-plasma treatment. b) XPS scan on the Au stripes from X_1 to X_3 by focusing on the Au $4f_{5/2}$ and $4f_{7/2}$ peaks.

In summary, we demonstrated a simple, high-yield route to hierarchical assembly of micelles composed of amphiphilic diblock copolymer over large areas by combining a top-down CESA in the cylinder-on-Si geometry at the microscopic scale with a bottom-up spontaneous self-assembly of diblock copolymer micelles at the nanometer scale. More importantly, hierarchical arranged inorganic nanoparticles can also be crafted by CESA of amphiphilic diblock copolymer/precursor solution, followed by exposure to oxygen plasma. This technique may offer a versatile way of producing a large variety of hierarchical structures, composed of functional block copolymers and nanocrystals, eliminating the need for costly, multistep lithography techniques.

Experimental Section

CESA of PS-b-P4VP toluene solution in the cylinder-on-Si geometry: Poly(styrene)-*block*-poly(4-vinylpyridine) (PS-*b*-P4VP; number average molecular weight M_n of PS = 41.0 kg mol^{-1} and P4VP = 24.0 kg mol^{-1}; polydispersity index, PDI = 1.09; Polymer Source Inc.) was dissolved in toluene at a concentration of 0.1 mg mL^{-1} and purified with a 200 nm poly(tetrafluoroethylene) (PTFE) filter. The cylindrical lens (L = 9.5 mm, H = 4.0 mm, W = 11.0 mm; Figure 1 a) and Si substrate were used as the upper and lower surfaces, respectively, to construct the cylinder-on-Si geometry. The Si substrate was cleaned with a mixture of sulfuric acid and Nochromix, then rinsed extensively with deionized water and blow dried with N_2. The contact of the cylinder with Si was made using a computer-programmable inchworm motor with a step motion on the micrometer scale. The cylinder-on-Si geometry was placed in a sealed chamber to minimize possible air convection and maintain a constant temperature during the evaporation process.

Surface reconstruction using solvent-vapor annealing: The regular PS-*b*-P4VP patterns formed on the Si substrate were exposed to tetrahydrofuran (THF) vapor for 6 h in a closed vessel to achieve morphological reconstruction of PS-*b*-P4VP. A small piece of gauze soaked with THF solvent was placed into a 33 cm^3 vessel. The vessel was sealed with Teflon and placed in an argon glove box to avoid temperature and humidity variation.

Preparation of gold nanoparticles in block copolymer micelles: Tetrachloroauric acid ($HAuCl_4 \cdot 3H_2O$) obtained from Sigma was used as received. $HAuCl_4 \cdot 3H_2O$ was added into the PS-*b*-P4VP toluene solution at the molar ratio of Au^{3+}/P4VP blocks = 0.1. The resulting solution was stirred for more than 72 h, allowing the Au^{3+} ions to migrate into the P4VP cores and coordinate with the pyridine groups of P4VP. The polymer template was then removed by oxygen plasma (Harrick Plasma; PDC-001) at 30 W and 300 mTorr for 45 minutes.

Characterization: The structures produced on the Si substrate were characterized by optical microscope (Olympus BX51, in reflection mode) and atomic force microscopy (Dimension 3100 (Digital Instruments) scanning force microscope in tapping mode). Vista probes (T190) with spring constants of 48 N m^{-1} were used as scanning probes. X-ray photoelectron spectroscopy (PHI 5500) measurements were performed with an Al standard x-ray source (1486.6 eV). The samples were attached to the holder using double stick tape to isolate the charging effects. The formation of nanoparticles was also examined by field-emission scanning electron microscope (FEI Quanta 250) operating at 20 kV under high vacuum.

Received: October 1, 2012
Published online: November 7, 2012

Keywords: amphiphilic block copolymers · hierarchical assembly · micelles · nanoparticles · self-assembly

[1] a) H. O. Jacobs, G. M. Whitesides, *Science* **2001**, *291*, 1763; b) T. Thurn-Albrecht, J. Schotter, C. A. Kastle, N. Emley, T. Shibauchi, L. Krusin-Elbaum, K. Guarini, C. T. Black, M. T. Tuominen, T. P. Russell, *Science* **2000**, *290*, 2126.
[2] Y. Lin, A. Boker, J. He, K. Sill, H. Xiang, C. Abetz, X. Li, J. Wang, T. Emrick, S. Long, Q. Wang, A. Balazs, T. P. Russell, *Nature* **2005**, *434*, 55.
[3] C. J. Hawker, T. P. Russell, *MRS Bull.* **2005**, *30*, 952.
[4] L. F. Zhang, A. Eisenberg, *Science* **1995**, *268*, 1728.
[5] a) S. Park, J. Y. Wang, B. Kim, J. Xu, T. P. Russell, *ACS Nano* **2008**, *2*, 766; b) B. Y. Kim, S. J. Park, T. J. McCarthy, T. P. Russell, *Small* **2007**, *3*, 1869; c) Y. Wang, M. Becker, L. Wang, J. Liu, R. Scholz, J. Peng, U. Gösele, S. Christiansen, D. H. Kim, M. Steinhart, *Nano Lett.* **2009**, *9*, 2384.
[6] a) S. Park, J. Y. Wang, B. Kim, T. P. Russell, *Nano Lett.* **2008**, *8*, 1667; b) W. L. Leong, P. S. Lee, A. Lohani, Y. M. Lam, T. Chen, S. Zhang, A. Dodabalapur, S. G. Mhaisalkar, *Adv. Mater.* **2008**, *20*, 2325.
[7] a) T. P. Bigioni, X.-M. Lin, T. T. Nguyen, E. I. Corwin, T. A. Witten, H. M. Jaeger, *Nat. Mater.* **2006**, *5*, 265; b) E. Rabani, D. R. Reichman, P. L. Geissler, L. E. Brus, *Nature* **2003**, *426*, 271.
[8] a) S. W. Hong, J. Xu, Z. Q. Lin, *Nano Lett.* **2006**, *6*, 2949; b) S. W. Hong, J. F. Xia, M. Byun, Q. Z. Zou, Z. Q. Lin, *Macromolecules* **2007**, *40*, 2831; c) S. W. Hong, S. Giri, V. S. Y. Lin, Z. Q. Lin, *Chem. Mater.* **2006**, *18*, 5164; d) S. W. Hong, J. F. Xia, Z. Q. Lin, *Adv. Mater.* **2007**, *19*, 1413; e) J. Xu, J. F. Xia, Z. Q. Lin, *Angew. Chem.* **2007**, *119*, 1892; *Angew. Chem. Int. Ed.* **2007**, *46*, 1860; f) J. Xu, J. F. Xia, S. W. Hong, Z. Q. Lin, F. Qiu, Y. L. Yang, *Phys. Rev. Lett.* **2006**, *96*, 066104; g) M. Byun, W. Han, F. Qiu, N. B. Bowden, Z. Q. Lin, *Small* **2010**, *6*, 2250; h) M. Byun, R. L. Laskowski, M. He, F. Qiu, M. Jeffries-El, Z. Q. Lin, *Soft Matter* **2009**, *5*, 1583; i) W. Han, Z. Lin, *Angew. Chem.* **2012**, *124*, 1566; *Angew. Chem. Int. Ed.* **2012**, *51*, 1534; j) M. Byun, N. B. Bowden, Z. Lin, *Nano Lett.* **2010**, *10*, 3111; k) M. Byun, S. W. Hong, F. Qiu, Q. Z. Zou, Z. Q. Lin, *Macromolecules* **2008**, *41*, 9312; l) M. Byun, J. Wang, Z. Q. Lin, *J. Phys. Condens. Matter* **2009**, *21*, 264014; m) W. Han, M. Byun, Z. Lin, *J. Mater. Chem.* **2011**, *21*, 16968; n) W. Han, M. Byun, L. Zhao, J. Rzayev, Z. Lin, *J. Mater. Chem.* **2011**, *21*, 14248.
[9] a) H. S. Kim, C. H. Lee, P. K. Sudeep, T. Emrick, A. J. Crosby, *Adv. Mater.* **2010**, *22*, 4600; b) H. Yabu, M. Shimomura, *Adv. Funct. Mater.* **2005**, *15*, 575.
[10] M. Abkarian, J. Nunes, H. A. Stone, *J. Am. Chem. Soc.* **2004**, *126*, 5978.
[11] a) S. Förster, M. Antonietti, *Adv. Mater.* **1998**, *10*, 195; b) B. H. Sohn, J. M. Choi, S. I. Yoo, S. H. Yun, W. C. Zin, J. C. Jung, M. Kanehara, T. Hirata, T. Teranishi, *J. Am. Chem. Soc.* **2003**, *125*, 6368; c) Z. Li, W. Zhao, Y. Liu, M. H. Rafailovich, J. Sokolov, K. Khougaz, A. Eisenberg, R. B. Lennox, G. Krausch, *J. Am. Chem. Soc.* **1996**, *118*, 10892.
[12] a) S. Förster, M. Zisenis, E. Wenz, M. Antonietti, *J. Chem. Phys.* **1996**, *104*, 9956; b) S. I. Yoo, B. H. Sohn, W. C. Zin, J. C. Jung, C. Park, *Macromolecules* **2007**, *40*, 8323.
[13] S. H. Yun, S. Il Yoo, J. C. Jung, W. C. Zin, B. H. Sohn, *Chem. Mater.* **2006**, *18*, 5646.
[14] Z. Q. Chen, C. C. He, F. B. Li, L. Tong, X. Z. Liao, Y. Wang, *Langmuir* **2010**, *26*, 8869.
[15] a) S. I. Yoo, B. H. Sohn, W. C. Zin, S. J. An, G. C. Yi, *Chem. Commun.* **2004**, 2850; b) S. I. Yoo, J. H. Kwon, B. H. Sohn, *J. Mater. Chem.* **2007**, *17*, 2969.
[16] M. Antonietti, E. Wenz, L. Bronstein, M. Seregina, *Adv. Mater.* **1995**, *7*, 1000.
[17] J. P. Spatz, S. Mossmer, C. Hartmann, M. Moller, T. Herzog, M. Krieger, H. G. Boyen, P. Ziemann, B. Kabius, *Langmuir* **2000**, *16*, 407.

